13th International Workshop on ECR Ion Sources,
College Station, TX, Feb. 26-28, 1997

ECR-based Atomic Collision Physics Research at ORNL

F.W. Meyer, M.E. Bannister, J.W. Hale, C.C. Havener, O. Woitke, and Q. Yan
Physics Division, Oak Ridge National Laboratory,
Oak Ridge, TN 37831-6372

After a brief summary of the present capability and configuration of the ORNL Multicharged Ion Research Facility (MIRF), and of upcoming upgrades and expansions, the presently on-line atomic collisions experiments are described. In the process, the utility of intense, cw ion beams extracted from ECR ion sources for low-signal rate experiments is illustrated.

Introduction

Since the last report on ORNL MIRF at the 1990 ECR workshop in Knoxville [1], the facility has seen a steady growth both in terms of the production capability for multicharged ion (MCI) beams and in terms of the range and individual capabilities of the atomic collisions experiments on-line in the facility. With the installation of a 10GHz CAPRICE ECR ion source in 1992, significant increases in ion beam intensities and attainable charge states were realized. For example, compared to the first-generation ORNL ECR source [2], the improvement in extracted Ar^{17+} beam intensity from the CAPRICE ECR source amounted to almost 6 orders of magnitude (corresponding to a current on the order of 1 nA), while Ar^{18+} (not measurable with the ORNL ECR source) increased to roughly 30 pA. The addition of a mini-oven [3] in the rf coaxial injection line of CAPRICE the following year greatly expanded the range of elements for which MCI beams could be produced. By either direct vaporization for lower melting point metals, or the use of more volatile metallic compounds for those species requiring, in pure form, temperatures higher than 1200 °C to attain adequate vapor pressure, the mini-oven could be used to generate MCI beams for virtually any element in the period table. This is illustrated in Fig. 1, which shows charge state distributions obtained for Pb and Mo beams, using direct heating of the pure material and the volatile metallic oxide MoO_3, respectively.

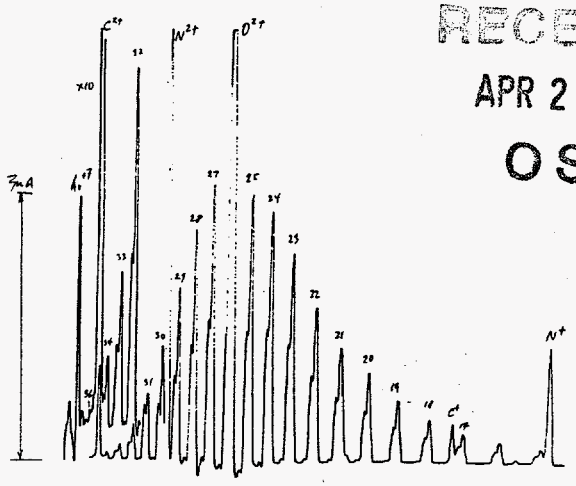

Lead Ion Charge State Distribution

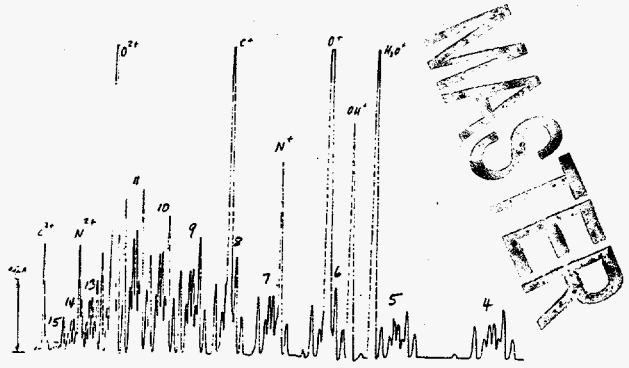

Molybdenum Ion Charge State Distribution

Fig. 1. CSD distributions of CAPRICE metallic ion beams extracted at 10 kV source potential, using mini-oven. The peaks denoted by numbers correspond to Pb and Mo charge states, respectively.

In FY1997 a capital equipment project was approved for the installation of a 250 kV high voltage platform, for use in conjunction with the present CAPRICE source. In addition to expanding the capabilities of the present on-line experiments, availability of higher energy MCI beams will also make possible new classes of experiments that have so far been unexplored. As part of the same project, a second source with standard 25 kV isolation will be installed in our facility, aimed at extending the availability of very low energy MCI beams, utilizing a floating beamline approach similar to that employed at HMI-Berlin [4], by which keV-energy beams can be transported with high efficiency, and then decelerated to a few q × eV upon entry into various experimental chambers at ground potential. Between the two sources, a very broad energy range of almost 5 orders of magnitude will thus be accessible to the various experiments.

DISCLAIMER

ORNL MULTICHARGED ION RESEARCH FACILITY (MIRF)

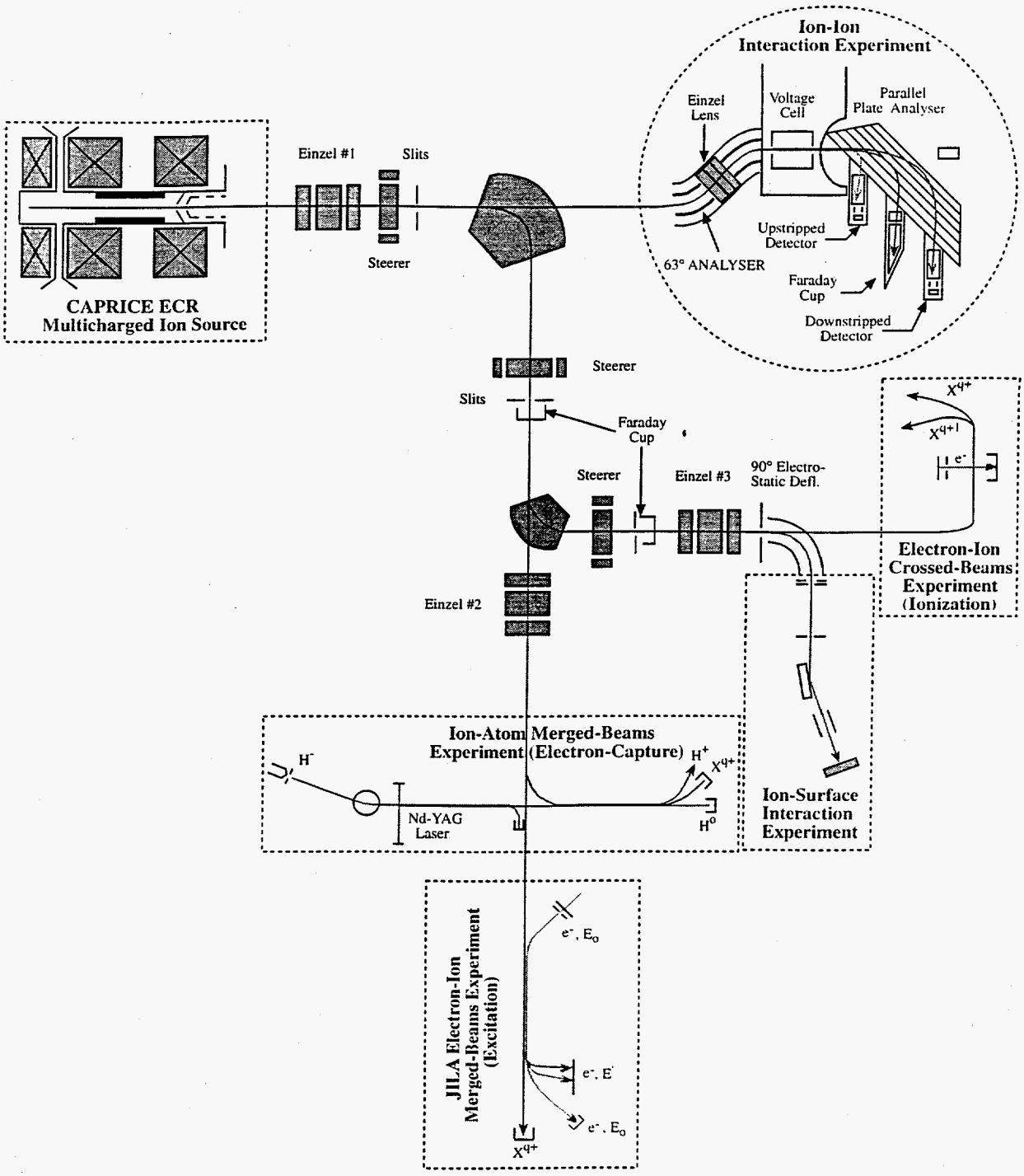

Fig. 2. Schematic lay-out of ORNL MIRF, and presently on-line experiments.

Figure 2 shows the schematic lay-out of ORNL MIRF. In the following sections brief summaries are given of the five atomic collisions experiments presently on-line.

Electron-ion Collisions

The electron-ion crossed beams apparatus (see Fig. 2) is used to measure electron ionization cross sections for ions in charge states 1-16, and also electron impact dissociation of molecular ions. Typical experimental parameters [5] are summarized in Table I. Focusing on the collimated beam intensity of Ni^{14+} transported through the apparatus shown in the last column, and the signal rate (i.e., Ni^{15+} count rate) resulting from electron impact ionization collisions with roughly 10 mA electron beam intercepting the MCI beam, it is seen that only roughly 1 in every 10^9 MCI will generate a "signal" event. Such low conversion efficiencies place severe requirements on incident ion beam intensities, which ECR ion sources are well suited to meet, and, of course, on the chamber vacuum (which is typically 10^{-10} T scale for all the experiments presently on-line), to minimize ionization events on residual gas. The utility of this crossed beams apparatus to study indirect mechanisms leading to ionization of MCI has been discussed previously [6]. Of equal utility is its ability to characterize metastable content in MCI beams used in other MIRF experiments. Knowledge of the initial quantum state of the MCI is crucial to the determination of accurate electron impact excitation cross sections, and is also important in the determination of reliable heavy particle electron capture cross sections, both of which are discussed further in the paragraphs below. Figures 3 and 4 illustrate the signature of MCI metastable content, namely non-zero cross section below the ground-state threshold, and give typical values of the metastable fractions for He-like and Mg-like MCI deduced from the data.

The other experiment studying electron collisions utilizes the merged electron ion beams energy loss (MEIBEL) technique [7] to determine

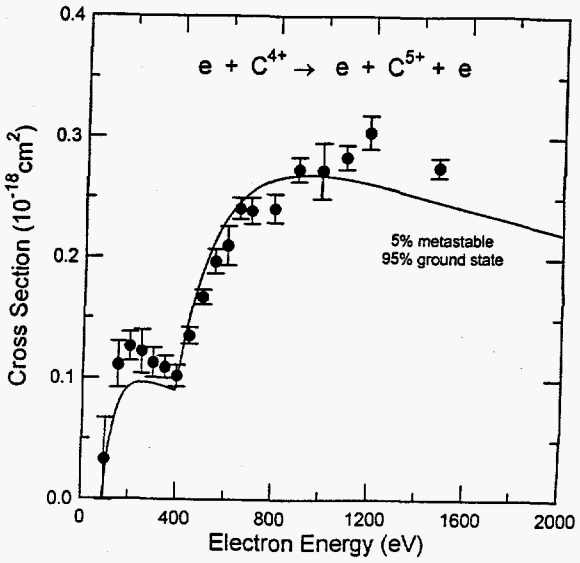

Fig. 3. Electron impact ionization cross section for ground state and metastable C^{4+} vs. electron energy.

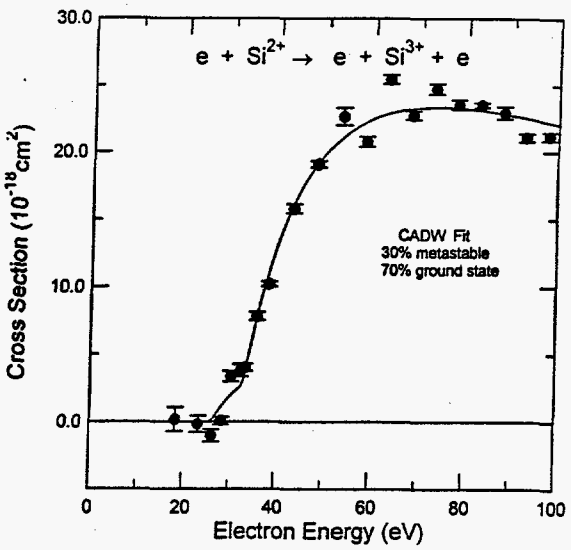

Fig. 4. Electron impact ionization cross section for ground state and metastable Si^{2+} vs. electron energy.

Table 1. Typical experimental parameters.

Parameter	Ni^{5+}	Ni^{6+}	Ni^{7+}	Ni^{8+}	Ni^{12+}	Ni^{14+}
Electron energy (eV)	300	400	500	600	1000	1300
Electron current (mA)	1.9	2.9	4.0	6.0	9.6	12.9
Ion current (particle nA)	2.3	2.4	1.0	1.8	3.2	0.2
Background count rate (Hz)	75	30	37	43	157	11.6
Signal count rate (Hz)	147	119	49	76	34	1.8

near-threshold absolute electron impact excitation cross sections. Conceived and developed at JILA, the apparatus was brought on-line in the facility in early 1990, as part of a continuing ORNL-JILA collaboration. In the MEIBEL technique, an electron beam is merged with the selected MCI beam using crossed electric and magnetic fields and allowed to interact over a roughly 65 mm electric-field-free region. A second E × B analyzer demerges the primary electron beam and the inelastically scattered electrons from the MCI beam, for subsequent detection in a Faraday cup and position sensitive detector, respectively. From the measured overlap of the two beams in the interaction region, the count rate of those electrons having lost a characteristic amount of energy (corresponding to the energy difference between initial and excited electronic states of the MCI) and the primary electron and MCI beam intensities, absolute electron impact excitation cross sections are determined. Figures 5 and 6 illustrate recent experimental results [8] for excitation of optically forbidden transitions in Mg-like Ar^{6+} and Zn-like Kr^{6+}, both showing strong resonance structures due to di-electronic recombination to intermediate excited states, which subsequently Auger decay to the final excited state of interest. Calculation of such resonances poses a severe challenge to atomic structure theory, and at present relies heavily on experimental measurements such as those shown for benchmarking and validation.

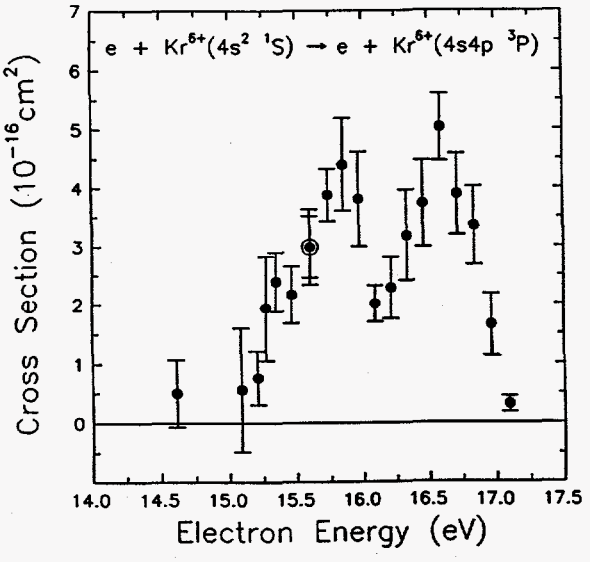

Fig. 5. Electron impact excitation cross section of Kr^{6+} vs. electron energy.

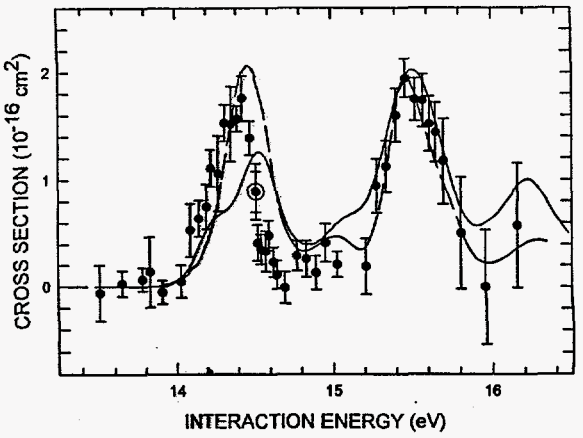

Fig. 6. Electron impact excitation cross section of Ar^{6+} vs. electron energy.

Heavy Particle Electron Transfer Collisions

A second merged beams apparatus, located immediately upstream of the MEIBEL experiment (see Fig. 2), is used to study electron capture by MCI in very low energy collisions with atomic hydrogen. In this experiment, a fast ground state atomic hydrogen beam, formed by photodetachment of H^-, is merged with a well-collimated MCI beam over a 47-cm interaction region. The protons produced by electron capture collisions with MCI are separated from the primary beams in a demerging magnet and subsequently counted. By judicious setting of the source high voltage, the MCI beam velocity relative to the fast H beam can be made extremely small, permitting determination of electron capture cross sections at energies as low as 10^{-2} eV/amu. Typical recent results [9] of such measurements are shown in Fig. 7 for N^{2+} + H collisions. Since the effective target thickness presented by the partner beam essentially decreases linearly with decreasing relative velocity of the two beams, sufficient MCI beam intensity becomes an increasingly important issue at the very lowest collision energies, and lack thereof becomes the main contributor to the larger uncertainties of the cross sections in that energy region. In addition to the large range of energies spanned by the measurements shown in the figure (almost 5 orders of magnitude!), illustrating one of the strengths of the merged beams technique, there is an interesting discrepancy apparent between the merged beams results for this system and previous results using an atomic hydrogen dissociation furnace in a narrow energy region between 200 and 2000 eV. This difference is ob-

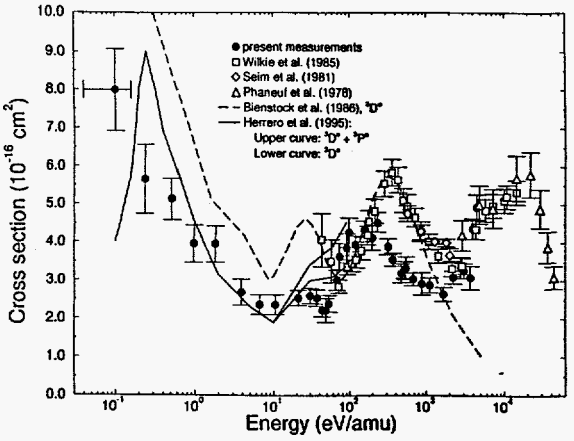

Fig. 7. Electron capture cross section for N^{2+} colliding with D, as function of collision energy.

served for other systems as well, and may point to possible limitations of the gas furnace technique, due to difficulties in correcting for collisions with undissociated but vibrationally excited H_2 still present in the furnace at high temperatures.

Since electron capture by MCI occurs almost exclusively at avoided crossings of the quasi-molecular potential curves and results in two charged collision products, there is usually a resulting energy gain, unique to each particular final state, that is shared between the two collision partners in such a way as to conserve energy and momentum in the center of mass frame. If the neutral H beam is chosen to be the faster of the two beams, then the H^+ product of the capture collision will experience an amplified energy increase in the laboratory frame due to the finite velocity of the center of mass frame. By use of a multi-grid energy filter after the demerging magnet, H^+ product ions correlated with different final excited states of the MCI can be distinguished. Such an energy filter has recently [10] been implemented. Figure 8 shows initial results of state-selective electron capture for Si^{4+} + D collisions obtained using such an approach.

The other experiment investigating heavy particle electron capture collisions is a recently developed self-merged beams experiment, which uses the unanalyzed beam (i.e., not separated by q/m) extracted from the ECR source to study intra-beam electron transfer between different charge states of the same atomic species, i.e. symmetric, non-resonant reactions of the kind $X^{a+} + X^{b+} \rightarrow X^{(a+1)+} + X^{(b-1)+}$. The experiment utilizes the fact that, for a given source voltage, ions with different charge states comprising the extracted beam travel at different velocities and can therefore undergo inelastic collisions with each other. A well-defined interaction region is established in a region labeled by high negative voltage. This has the dual advantage of permitting discrimination, using energy analysis, against beam-beam charge transfer events occurring upstream of the experiment, and increasing the dispersion of the two collision products, since the product ion having captured an electron experiences a net energy gain traversing the voltage cell, while the one giving up the electron experiences a net energy loss. In the parallel plate energy analyzer downstream of the voltage cell (see Fig. 2), the collision products thus have a greater spatial separation from each other, and, more importantly, from the primary beams (all having the same E/q) as well. Coincident detection of the two collision products is employed to discriminate against unwanted background events due to collisions with residual gas. This is an ambitious experiment, due in part to the presence of the spectator beams, whose only contribution is to increase the background rate, and in part due to the strong differential focusing of the labeling cell at the voltages required for the measurements, and is presently still in the testing phase. Efforts are still underway to observe the beam-beam charge exchange signature (i.e., coincidence peak), but proper "singles" operation of the upstripped channel has been verified

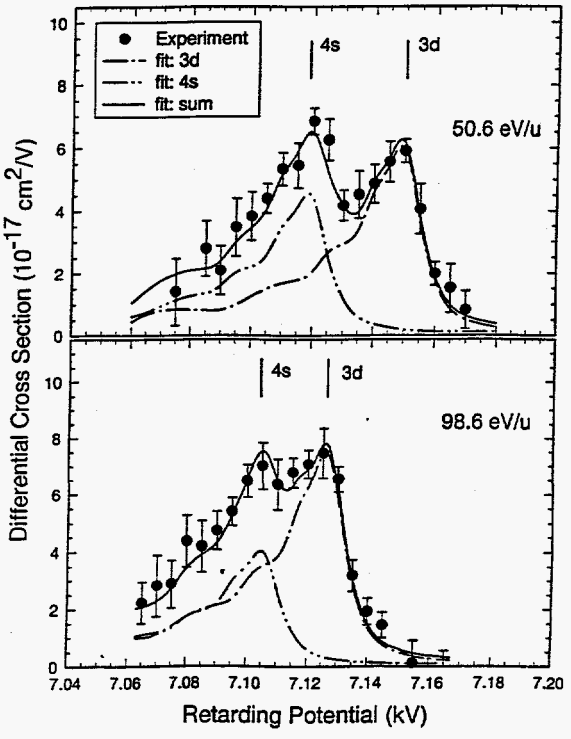

Fig. 8. State-selective electron capture cross section for Si^{4+} colliding with D, at two different collision energies.

by measurement [11] of the stripping cross section for He^{2+} in Ar, which, as can be seen from Fig. 9, is in reasonable agreement with the trend established by previous measurements at higher collision energies.

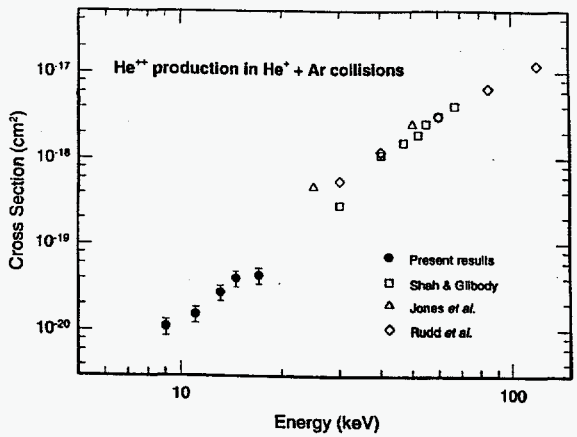

Fig. 9. Stripping cross section for He^{2+} in Ar vs. projectile energy.

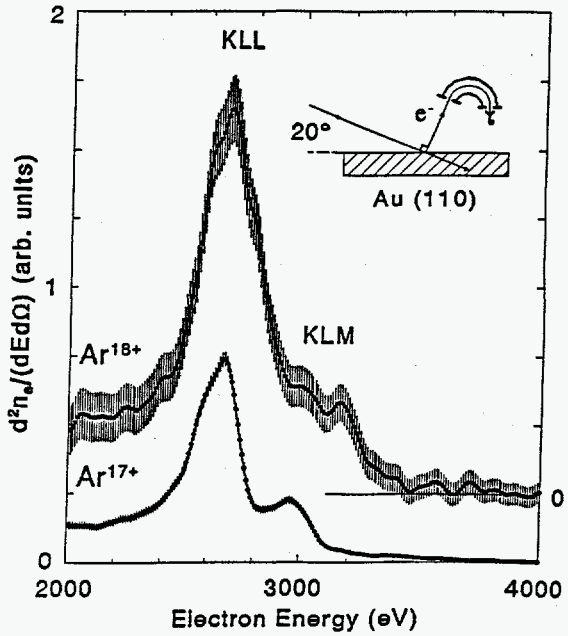

Fig. 10. Ar K-Auger electron spectra for 20 kV × q Ar^{17+} and Ar^{18+} projectiles incident on Au(110).

MCI-surface Interactions

Investigations of electron emission during grazing MCI-surface interactions via electron spectroscopy and total yield measurements have been carried out at MIRF for more than ten years. Figure 10 shows measurements of K-Auger electron spectra for Ar^{17+} and Ar^{18+} incident on Au(110) made shortly after installation of the new CAPRICE ECR source. From such spectra, the number of electrons in the projectile L shell at the time of the K-Auger decay can be deduced [12]. Using the known lifetimes for Auger decay, L-shell neutralization rates can thus be determined, providing insights into neutralization processes occurring in such interactions.

More recently studies of projectile scattering were initiated [13] which focused on obtaining complementary information on neutralization timescales and mechanisms relevant to grazing MCI-surface interactions. Using a position sensitive detector some distance away from the single crystal target, angular distributions of scattered projectiles can be measured, permitting determination, for example, of the acceleration of the MCI prior to impact on the surface by virtue of the attraction towards its own image charge. This image charge acceleration causes a measurable increase of the projectile incidence angle on the surface, which, at the grazing incidence conditions (i.e., specular reflection conditions) of the measurements translates into a measurable increase of the projectile reflection angle, since the scattered projectile leaves the surface almost completely neutralized (i.e., no corresponding image charge interactions on the receding trajectory). Figure 11a shows the increase of scattering angles observed for different charge state Pb beams at a fixed geometric incidence angle of 0.8°, while Fig. 11b shows the corresponding projectile energy gains. The energy gain experienced by an MCI depends sensitively on how far above the surface the projectile is able to capture electrons on its approach trajectory, and how many, and is thus an excellent probe of above-surface neutralization processes.

Compared to the previous experiments described in this paper, the requirements on incident beam intensity are somewhat relaxed for the grazing incidence ion scattering measurements, since reflection coefficients are close to 100% and essentially all of the scattered ions are registered on the position sensitive detector. However, it must be kept in mind that in order to have the high angular resolution required, e.g. for the above energy gain measurements, the incident beams are tightly collimated to a divergence of less than 0.1° and diameter of less than 0.5 mm, so that only a small fraction of the beams extracted from the source is used for the measurement. In addition, for time resolved studies it is still important to have as high a count rate (consistent with the capabilities of the PSD, of course) as possible. This is illustrated in Fig. 12, which shows the change in channeling pattern observed for incident O^{7+} ions that occurs when the [2×1] [1×1]random phase transition in

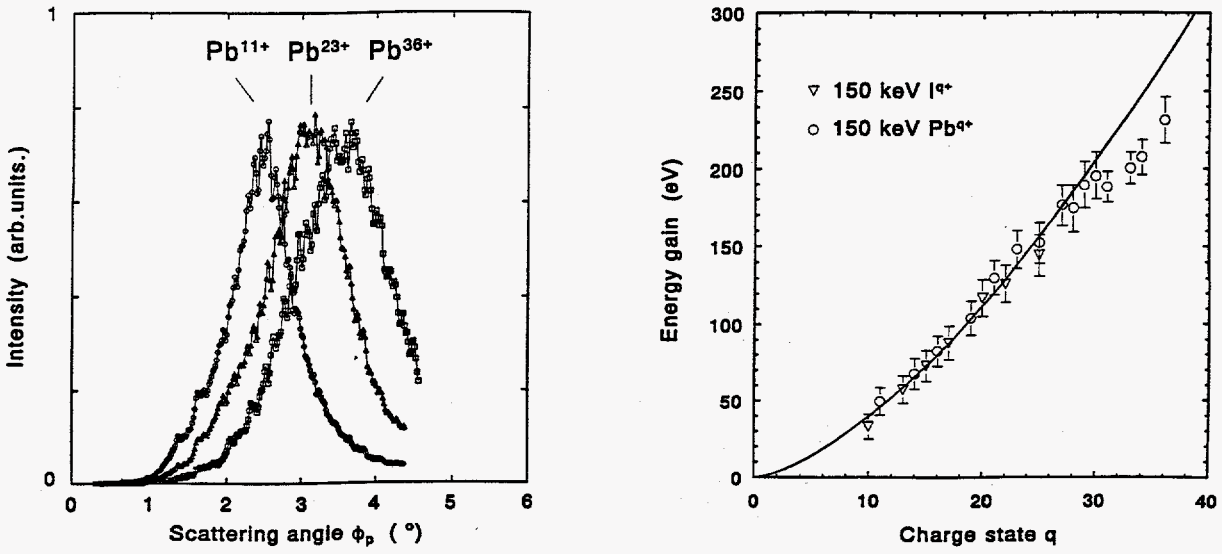

Fig. 11. a) Scattering angle distributions for 150 keV Pb ions for different incident charge states at fixed incidence angle; b) image acceleration energy gains experienced by MCI above a Au(110) surface as function of incident charge state q.

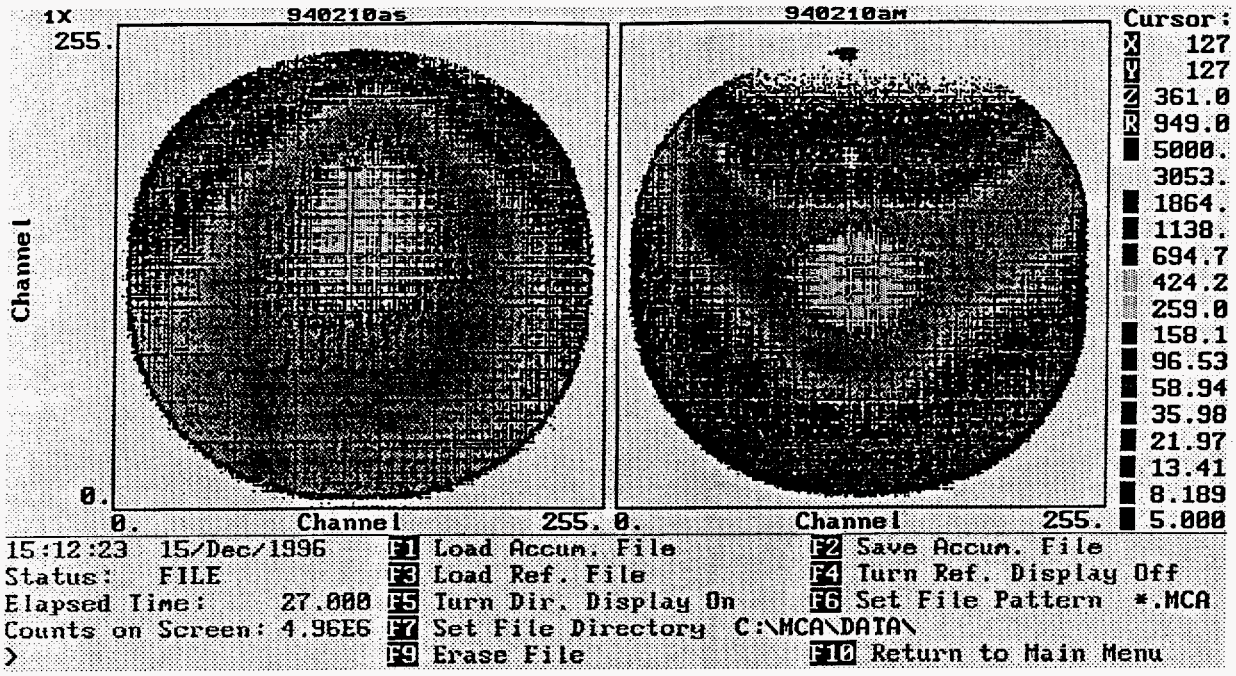

Fig. 12. Channeling patterns for scattering of 70 keV O^{7+} from Au(110) slightly above the surface reconstruction phase transition temperature of 650K (i.e., for [1 x 1] random surface reconstruction), and slightly below (i.e., for [2 x 1] "missing row" surface reconstruction).

Au(110) occurs at 650K. The two spectra were taken within 1 min of each other as the Au(110) sample cooled after annealing, and required less than 30s each, the first for a temperature slightly higher than the phase transition temperature, and the second slightly below.

Acknowledgments

It is a pleasure to thank the Grenoble team, particularly G. Melin and D. Hitz for excellent support and service of the ORNL CAPRICE source. The research reported in this paper was supported by the Division of Chemical Sciences, Office of Basic Energy Sciences, and Office of Fusion Energy Sciences, U.S. Department of Energy under contract No. DE-AC05-96OR22464 with Lockheed Martin Energy Research Corp.

References

[1] F.W. Meyer, R.A. Phaneuf, D.C. Gregory, C.C. Havener, J.W. Hale, P.A. Zeijlmans van Emmichoven, and J.S. Thompson, Proceedings of the 10th International Workshop on ECR Ion Sources, Knoxville, 1990, CONF-9011136, p. 367.

[2] F.W. Meyer, Proceedings of the 6th International Workshop on ECR Ion Sources, Berkeley, CA, 1985, PUB-5143, p. 37.

[3] D. Hitz, G. Melin, M. Pontonnier, and T.K. N'Guyen, Proceedings of the 11th International Workshop on ECR Ion Sources, Groningen, 1993, KVI-Report 996, p. 91.

[4] B. Martin, M. Grether, R. Köhrbrück, U. Stettner, and H. Waldmann, ibid, p. 188.

[5] L.J. Wang, K. Rinn, and D.C. Gregory, J. Phys. B 21, 2117 (1988).

[6] F.W. Meyer, International Conference on ECR Ion Sources and their Applications, East Lansing, 1987, NSCL Report No. MSUCP-47, p. 520.

[7] E.W. Bell et al., Phys. Rev. A 49, 4585 (1994).

[8] Y.-S. Chung, N. Djuric, B. Wallbank, G.H. Dunn, M.E. Bannister, and A.C.H. Smith, Phys. Rev. A 55, 2044 (1997); M.E. Bannister, X.Q. Guo, T.M. Kojima, and G.H. Dunn, Phys. Rev. Lett. 72, 3336 (1994).

[9] Marc Pieksma, M.E. Bannister, W.Wu, and C.C. Havener, Phys. Rev. A, April (1997).

[10] W. Wu and C.C. Havener. J. Phys. B Lett., to be published.

[11] J. Shinpaugh, F.W. Meyer. and S. Datz, Nucl. Instrum. Methods Physics Res. B99, 198(1995).

[12] F.W. Meyer, L. Folkerts, H.O. Folkerts, and S. Schippers, Nucl. Instrum. Methods Physics Res. B98, 441(1995).

[13] L. Folkerts, S. Schippers, and F.W. Meyer, Phys. Rev. Lett. 74, 2204 (1995).